Hydrogen-Bond Chemistry Inhibits Jahn-Teller Distortion Caused by Mn 3d Orbitals for Long-lifespan Aqueous Zn//MnO_2 Battery

Ziming Xu[a], Jiwei Wang[a], Wenyuan Zhang[a], Zhichen Shi[a], Yongbao Feng[a], Chenglong Liu[b], Huili Fu[c], Zhenzhong Yong[c], Qiulong Li[a]*

a. College of Materials Science and Engineering, Nanjing Tech University, Nanjing 211816, China

b. National Synchrotron Radiation Laboratory, University of Science and Technology of China, Hefei 230026, China

c. Key Laboratory of Multifunctional Nanomaterials and Smart Systems, Advanced Materials Division, Suzhou Institute of Nano-Tech and Nano-Bionics, Chinese Academy of Sciences, Suzhou, 215123, China

Corresponding Author: qlli@njtech.edu.cn (Q. Li)

Materials

Manganese sulfate monohydrate ($MnSO_4 \cdot H_2O$, 99%), sodium sulfate anhydrous (Na_2SO_4, 99%) and ammonium persulfate ($(NH_4)_2S_2O_8$, 98%) were purchased from Shanghai Aladdin Biochemical Technology Co., Ltd. Zinc sulfate heptahydrate ($ZnSO_4 \cdot 7H_2O$, 99.5%) and potassium permanganate ($KMnO_4$, AR) were purchased from Yonghua Chemical Co., Ltd. Boric acid (H_3BO_3, 99.8%) was obtained from Sinopharm Chemical Reagent, China. Carboxymethylcellulose sodium (CMC) was obtained from DodoChem. Super P (99%) was purchased Tianjin EVS Chemical Technology Co., Ltd. Polyvinylidene fluoride (PVDF, AR) was purchased from Shanghai Macklin Biochemical Co., Ltd. N-methyl-2-pyrrolidone (NMP, AR) was obtained from Sinopharm Chemical Reagent, China. Carbon cloth (CC-W0S1009) was purchased from Sinero. Absolute ethanol alcohol (CH_3CH_2OH) was from Wuxi Yasheng Chemical Company. Potassium permanganate ($KMnO_4$, 99%) was purchased from Shanghai Lingfeng Chemical Reagent Co., Ltd. Deionized water (H_2O) was RO grade water made by BioSafer pure water machine in the laboratory. Each of these chemicals was used directly without any further purification.

Preparation of the NHMO nanoflowers

The NHMO is prepared by a simple hydrothermal reaction. 1.896 g $KMnO_4$ was dissolved in 30 mL of deionized water to form solution A, then 0.338 g $MnSO_4 \cdot H_2O$ and 0.114 g $(NH_4)_2S_2O_8$ were dissolved in 30 mL of deionized water to obtain solution B. After solution A and solution B were fully mixed, solution A was slowly added to solution B to obtain a mixed solution. The mixed solution was transferred into a 100 mL Teflon-lined stainless-steel autoclave for reaction at 160 °C for 12 h. After cooling to room temperature, wash product with deionized water for three times and dried in a vacuum oven overnight. As a comparison, δ-MnO_2 was obtained through a same hydrothermal process but without the addition of $(NH_4)_2S_2O_8$.

Preparation of the NHMO and MnO_2 cathodes

Firstly, the cathode slurry was prepared by mixing NHMO or MnO_2 as the active material, super P as the electrical conductor and Polyvinylidene fluoride (PVDF) as the binder at a mass ratio of 7:2:1 in N-methyl-2-pyrrolidone solvent. Then, the obtained slurry was uniformly coated on the CC. Finally, the CC loaded with cathode slurry was dried overnight at 60 ^{o}C in a vacuum atmosphere to acquire the NHMO and MnO_2 cathodes. The mass loading of active material in each electrode disc is around 1.2-1.5 mg cm^{-2}.

Preparation of the Zn NSs/CC anode

The Zn NSs/CC anodes were prepared by electrochemical deposition with a three-electrode system. The CC, Pt sheet, and Ag/AgCl are the working, counter and reference electrodes, respectively. The aqueous electrolyte is prepared by mixing 6.25 g $ZnSO_4 \cdot 7H_2O$, 6.25 g Na_2SO_4 and 1 g H_3BO_3 in 50 mL deionized water. Finally, the Zn NSs/CC anode was prepared via electrochemical deposition at a current density of -40 mA cm^{-2} for 600 s. The average mass loading of Zn NSs on CC surface is about 6.64 mg cm^{-2}.

Preparation of $ZnSO_4$-CMC electrolyte

The $ZnSO_4$-CMC gel electrolyte was synthesized by dissolving 10 g $ZnSO_4 \cdot 7H_2O$, 0.5 g $MnSO_4 \cdot H_2O$ and 3 g CMC in 80 mL deionized water and stirring vigorously at 85 °C for 90 min.

Characterization

The morphologies of the as-fabricated samples were observed by scanning electron microscopy (SEM; Hitachi S-4800, 5 kV). The microstructures of the as-prepared samples were characterized by transmission electron microscopy (TEM; FEI Tecnai G2 F20 S-Twin) operating at an acceleration voltage of 200 kV. Raman spectra are collected using a Raman spectrometer (horiba evolution) to monitor molecular states and structures. The chemical compositions and phase structures of the as-

prepared samples were analyzed on an ESCALAB MKII X-ray photoelectron spectrometer (XPS) using non-monochromatized Mg Kα X-rays as the excitation source and a Rigaku D/MAX2500 V system using Cu Kα radiation (λ = 1.5418 Å) to obtain the X-ray diffraction (XRD) patterns. Fourier transform infrared spectroscopy (FT-IR) is used to analyze the chemical bond information of the sample (Nicolet iS10).

Electrochemical measurements

The electrochemical evaluation was carried out by assembling into a CR2032-type coin cell, using the NHMO wafer as a cathode, whatman GF/D glass fiber as a separator, Zn foil as anode and 2 M $ZnSO_4 \cdot 7H_2O$ with 0.2 M $MnSO_4 \cdot H_2O$ solution as the electrolyte. The CV and EIS were tested using an electrochemical workstation (CHI 760E). The GCD performance and GITT measurements are obtained through a battery testing system (Land 2001A) with a voltage ranging from 0.8 V to 1.8 V at 28 °C. MnO_2 used the same method to assemble batteries to test electrochemical performance. The capacity (C), energy density (E), and power density (P) were calculated according to the following equations:

$$C_A = \frac{I\Delta t}{3600A} \tag{1}$$

$$E_A = C_A \times V_P \tag{2}$$

$$P_A = 3600 \times \frac{E_A}{\Delta t} \tag{3}$$

Where A is the mass of active material in AZBs. I, Δt and V_p represent the discharge current, discharge time, and voltage platform, respectively.

GITT is used to calculate the ion diffusion coefficient (D), and D is calculated based on the following equation:

$$D = \frac{4}{\pi\tau}\left(\frac{m_B V_M}{M_B S}\right)^2\left(\frac{\Delta E_S}{\Delta E_\tau}\right)^2$$
$$= \frac{4}{\pi\tau}\left(\frac{m_B V}{n M_B S}\right)^2\left(\frac{\Delta E_S}{\Delta E_\tau}\right)^2$$
$$= \frac{4}{\pi\tau}\left(\frac{m_B}{\rho S}\right)^2\left(\frac{\Delta E_S}{\Delta E_\tau}\right)^2$$

where m_B, V_M and M_B are the mass (g), molar volume ($cm^3\ mol^{-1}$) and molar mass ($g\ mol^{-1}$) of the electrode, respectively. τ is the duration current pulse time (s), S is the contact area (cm^2) between electrode and electrolyte, ρ is the density of the active material ($g\ cm^{-3}$), ΔE_S is the voltage change between two adjacent equilibrium states, and ΔE_τ is the voltage change due to galvanostatic charging/discharging. A current density of 0.1 A g^{-1} is applied to the electrode with τ = 5 min and then stood for 30 min without current impulse.

According to the slope at the low frequency region in the EIS spectra, the ionic diffusion coefficient can be derived from the following formula:[1,2]

$$Z' = R_s + R_f + R_{ct} + \sigma_w \omega^{-0.5}$$

$$D = \frac{R^2T^2}{2A^2n^4F^4C^2\sigma_w^2}$$

Where R, T, A, n, F, C, and ω are the gas constant (8.314 J $mol^{-1}\cdot k^{-1}$), test temperature (301 K), electrode area, reactive electron number per chemical formula, Faraday's constant (96500 C mol^{-1}), the molar concentration of ions, and angular frequency, respectively. σ_w is the linear slopes from the relationship between frequencies and real part of impedance.

DFT calculations

First-principles calculations were performed within the density functional theory (DFT) framework, as implemented in the Vienna Ab initio Simulation Package (VASP) code. The study used the Perdew-Burke-Ernzerhof (PBE) function describe the electrons exchange-correlation potentials. In the calculation, we build 3 × 3 the vacuum layer of 20 Å is applied to each unit cell.

The Hubbard-type correction (Ueff = 4.0 eV) was applied to the 3d orbitals of Mn. The energy cutoff was 450 eV and the SCF tolerance was 1.0×10^{-6} eV per atom. The equilibrium lattice constants of MnO_2 unit cell were optimized when using a 5 × 5 × 2 Monkhorst Pack K-point grid for Brillouin zone sampling. The Brillouin zone integral utilized the surfaces structures of 3 × 3 × 1 Monkhorst Pack K-point sampling. The adsorption energies (E_{ads}) were calculated as $E_{ads} = E_{ad/sub} - E_{ad} - E_{sub}$, where $E_{ad/sub}$, E_{ad} and E_{sub} are the optimized adsorbate/substrate system, the adsorbate, and the clean substrate, respectively. The climbing-image nudged elastic band (CI-NEB) method was employed to calculate the Zn ion migration barrier The optimization was completed when the energy, maximum force displacement was smaller than 1.0×10^{-5} eV, 0.03 eV $Å^{-1}$.

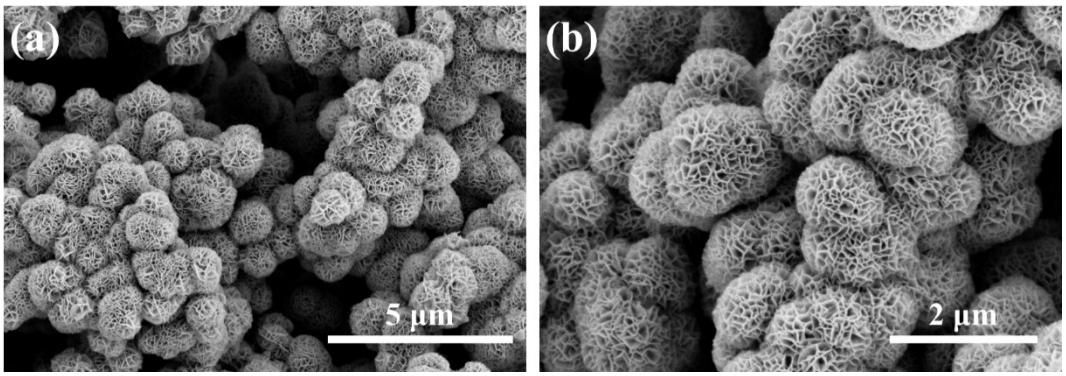

Figure S1. (a, b) SEM images of the NHMO at different magnifications.

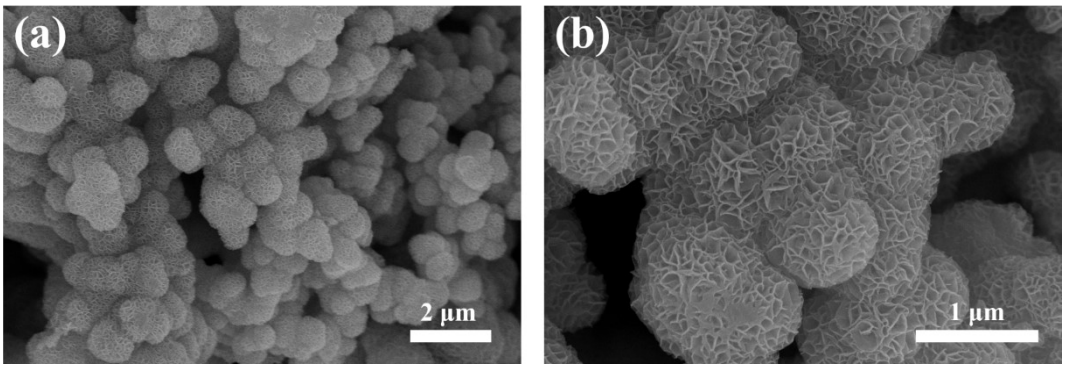

Figure S2. (a, b) SEM images of the MnO_2 at different magnifications.

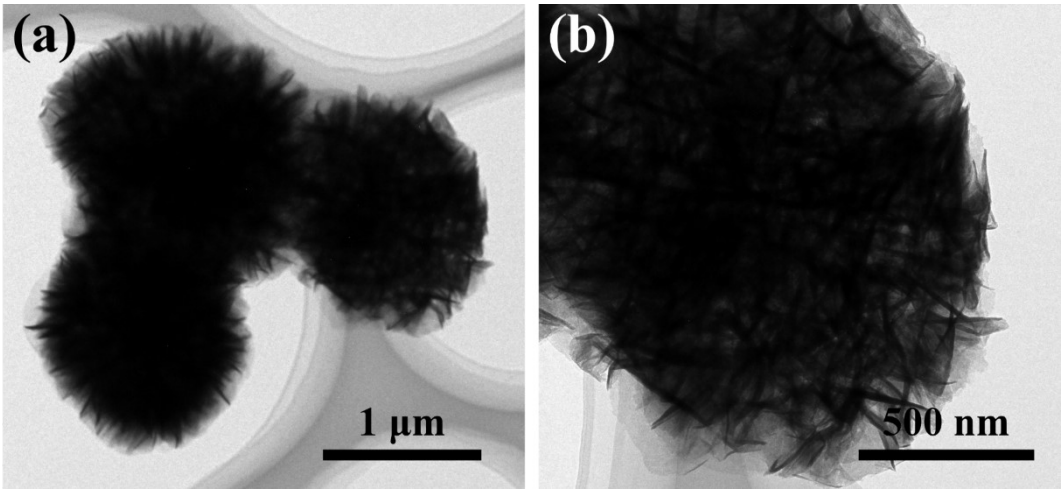

Figure S3. (a, b) TEM images of the NHMO at different magnifications.

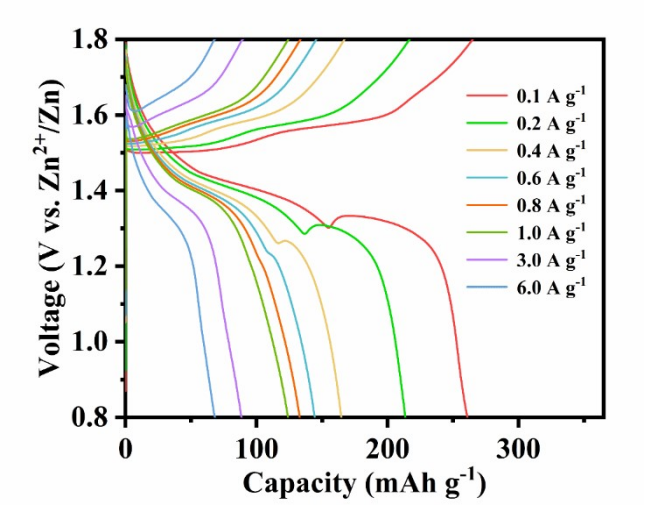

Figure S4. GCD curves of the MnO_2 electrode at different current densities.

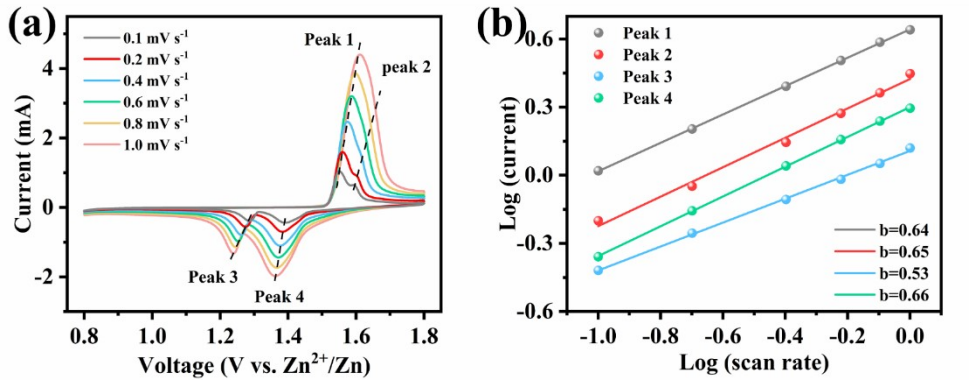

Figure S5. (a) CV curves the MnO_2 electrode at different scan rates ranging from 0.1 to 1.0 mV s^{-1}.

(b) The relationship between log(*i*) and log(*v*).

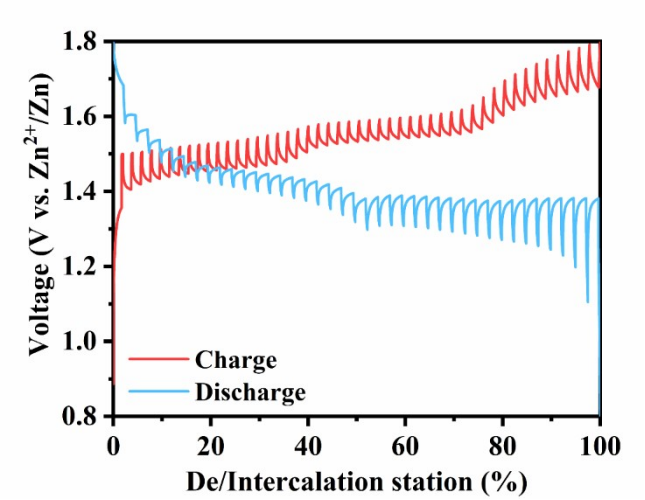

Figure S6. GITT curves of the MnO_2 electrode.

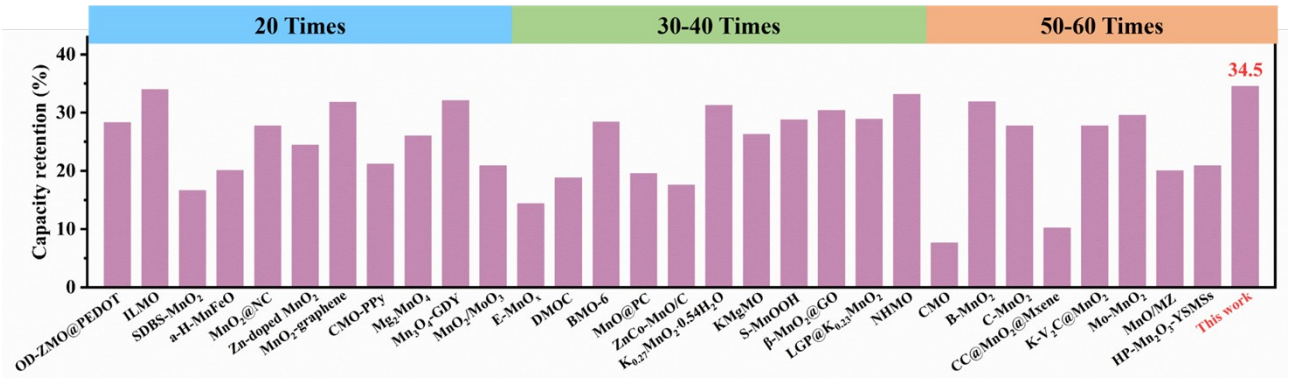

Figure S7. Comparison of the rate performance between the NHMO and previously reported manganese-based materials.[3-32]

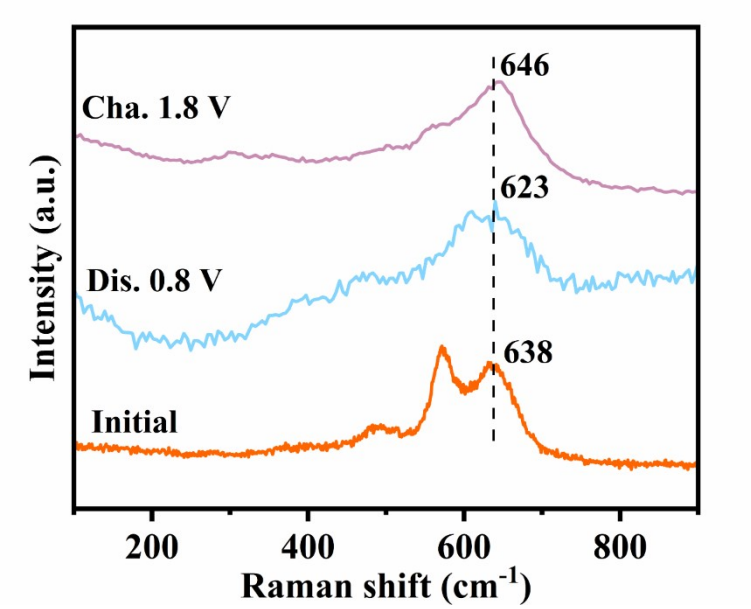

Figure S8. *Ex-situ* Raman spectra of the MnO_2 electrode.

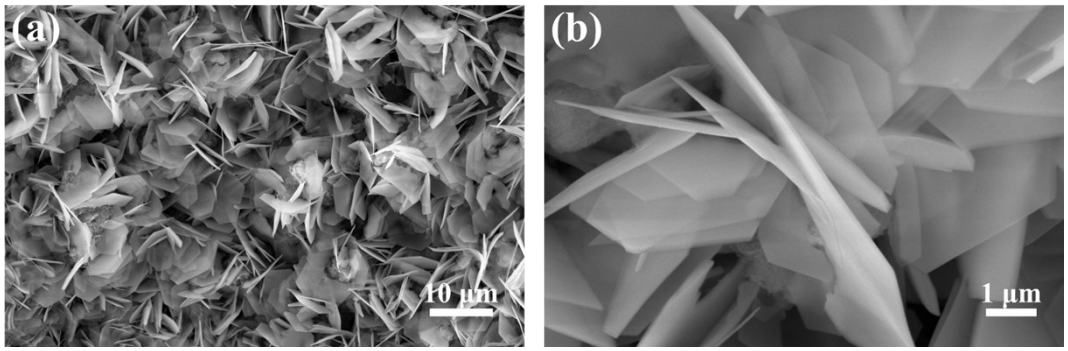

Figure S9. (a, b) SEM images of the NHMO electrode with different magnifications at discharge to 0.8 V.

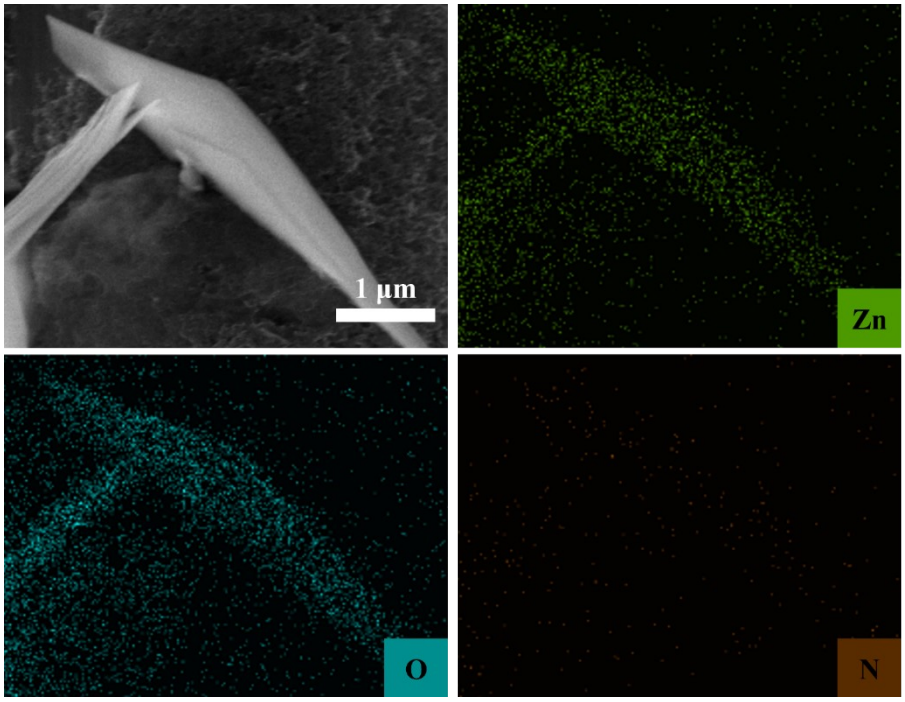

Figure S10. SEM image and EDX element mapping of ZHS.

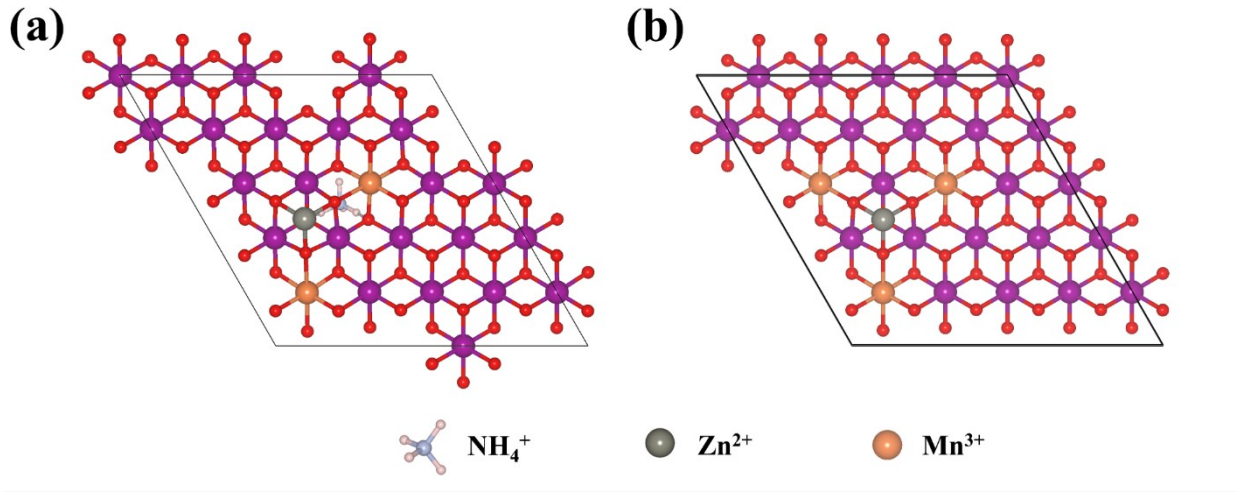

Figure S11. Schematic of the optimized structure of the NHMO (a) and MnO_2 (b) at the discharge phase.

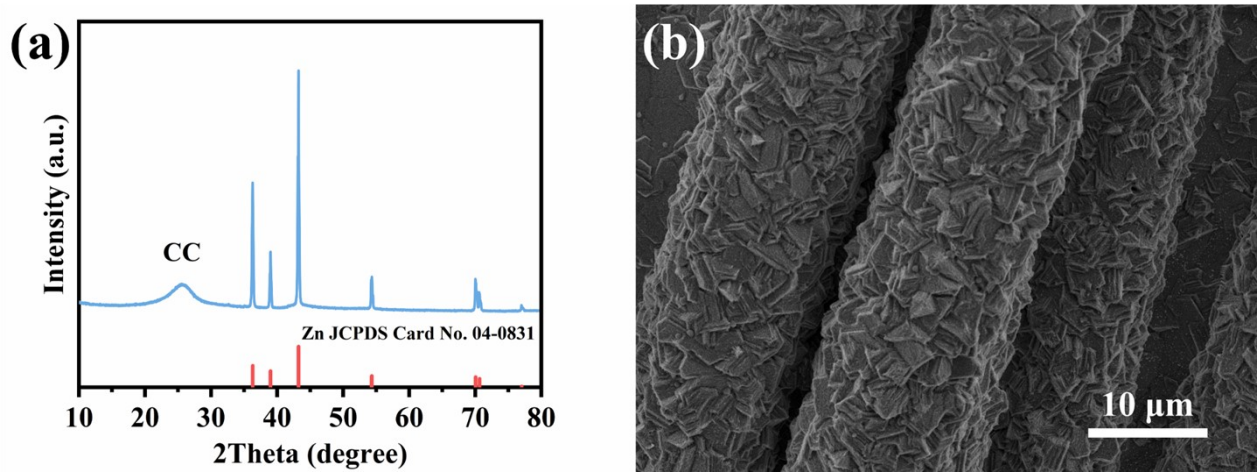

Figure S12. XRD pattern (a) and SEM image (b) of the Zn NSs/CC.

References:

1 C. Liu, Z. Neale, J. Zheng, X. Jia, J. Huang, M. Yan, M. Tian, M. Wang, J. Yang and G. Cao, *Energy Environ. Sci.*, 2019, **12**, 2273-2285.

2 S. Deng, Z. Tie, F. Yue, H. Cao, M. Yao and Z. Niu, *Angew. Chem. Int. Ed.*, 2022, **134**, e202115877.

3 L. Chen, Y. Dong, M. Han, T. Song, X. Zheng, W. He, B. Long, X. Wu, Y. Pei and X. Wang, *Chem. Eng. J.*, 2023, **473**, 145046.

4 S. Deng, B. Xu, X. Liu, C.-W. Kan and T. Chen, *Chem. Eng. J.*, 2023, **475**, 146098.

5 S. Ding, M. Zhang, R. Qin, J. Fang, H. Ren, H. Yi, L. Liu, W. Zhao, Y. Li, L. Yao, S. Li, Q. Zhao and F. Pan, *Nano-Micro Lett.*, 2021, **13**, 173.

6 X. Guo, H. Sun, C. Li, S. Zhang, Z. Li, X. Hou, X. Chen, J. Liu, Z. Shi and S. Feng, *J. Energy Chem.*, 2022, **68**, 538-547.

7 H.-b. He, Z. Liu, Z.-x. Luo, Z.-h. Zhang, Y. Chen and J. Zeng, *J. Alloys Compd.*, 2023, **960**, 170853.

8 W. Jiang, W. Wang, H. Shi, R. Hu, J. Hong, Y. Tong, J. Ma, C. Liang, J. Peng and Z. Xu, *J. Colloid Interface Sci.*, 2023, **647**, 124-133.

9 F. Jing, Y. Liu, Y. Shang, C. Lv, L. Xu, J. Pei, J. Liu, G. Chen and C. Yan, *Energy Storage Mater.*, 2022, **49**, 164-171.

10 F. Jing, C. Lv, L. Xu, Y. Shang, J. Pei, P. Song, Y. Wang, G. Chen and C. Yan, *J. Energy Chem.*, 2023, **87**, 314-321.

11 V. P. Joshi, N. Kumar, P. K. Pathak, M. S. Tamboli, N. T. N. Truong, C. D. Kim, R. S. Kalubarme and R. R. Salunkhe, *ACS Appl. Mater. Interfaces*, 2023, **15**, 24366-24376.

12 X. Li, Q. Zhou, Z. Yang, X. Zhou, D. Qiu, H. Qiu, X. Huang and Y. Yu, *Energy Environ. Mater.*,

2022, **6**, e12378.

13 Z. Li, Y. Zheng, Q. Jiao, Y. Zhao, H. Li and C. Feng, *Chem. Eng. J.*, 2023, **465**, 142897.

14 L. Liu, Y. C. Wu, L. Huang, K. Liu, B. Duployer, P. Rozier, P. L. Taberna and P. Simon, *Adv. Energy Mater.*, 2021, **11**, 2101287.

15 Y. Liu, Y. Ma, W. Yang, S. Bao, H. Chen and M. Xu, *Chem. Eng. J.*, 2023, **473**, 145490.

16 Y. Liu, Z. Qin, X. Yang and X. Sun, *Adv. Funct. Mater.*, 2021, **32**, 2106994.

17 Y. Liu, K. Wang, X. Yang, J. Liu, X.-X. Liu and X. Sun, *ACS Nano*, 2023, **17**, 14792-14799.

18 H. Luo, B. Wang, J. Jian, F. Wu, L. Peng and D. Wang, Mater. Today Energy, 2021, 21, 100799.

19 Y. Ma, M. Xu, R. Liu, H. Xiao, Y. Liu, X. Wang, Y. Huang and G. Yuan, *Energy Storage Mater.*, 2022, **48**, 212-222.

20 M. Qi, F. Li, Z. Zhang, Q. Lai, Y. Liu, J. Gu and L. Wang, *J. Colloid Interface Sci.*, 2022, **615**, 151-162.

21 K. Sun, Y. Shen, J. Min, J. Pang, Y. Zheng, T. Gu, G. Wang and L. Chen, *Chem. Eng. J.*, 2023, **454**, 140394.

22 Q. Sun, J. He, X. Li, T. Lu, W. Si, F. Zhao, K. Wang and C. Huang, *Chem. Eng. J.*, 2022, **432**, 134402.

23 T. Sun, S. Zheng, Q. Nian and Z. Tao, *Small*, 2022, **18**, 2107115.

24 J. Tan, T. Feng, S. Hu, Y. Liang, S. Zhang, Z. Xu, H. Zhou and M. Wu, *Appl. Surf. Sci.*, 2022, **604**, 154578.

25 C. Wang, Y. Zeng, X. Xiao, S. Wu, G. Zhong, K. Xu, Z. Wei, W. Su and X. Lu, *J. Energy Chem.*, 2020, **43**, 182-187.

26 Y. Xu, G. Zhang, J. Zhang, X. Wang, J. Wang, S. Jia, Y. Yuan, X. Yang, K. Xu, C. Wang, K. Zhang, W. Li and X. Li, *J. Colloid Interface Sci.*, 2023, **652**, 305-316.

27 X. Yuan, T. Sun, S. Zheng, J. Bao, J. Liang and Z. Tao, *J. Mater. Chem. A*, 2020, **8**, 22686-22693.

28 H. Zhang, J. Wang, Q. Liu, W. He, Z. Lai, X. Zhang, M. Yu, Y. Tong and X. Lu, *Energy Storage Mater.*, 2019, **21**, 154-161.

29 W. Zhao, J. Fee, H. Khanna, S. March, N. Nisly, S. J. B. Rubio, C. Cui, Z. Li and S. L. Suib, *J. Mater. Chem. A*, 2022, **10**, 6762-6771.

30 Z. Zheng, G. Yang, J. Yao, J. Li, J. Zheng, Z. Wu, Y. Gan, C. Wang, L. Lv, H. Wan, C. Chen, H. Wang, L. Tao, J. Zhang and H. Wang, *Appl. Surf. Sci.*, 2022, **592**, 153335.

31 X. Zhu, Z. Cao, W. Wang, H. Li, J. Dong, S. Gao, D. Xu, L. Li, J. Shen and M. Ye, *ACS Nano*, 2021, **15**, 2971-2983.

32 R. Zou, Z. Tang, X. Chen, Z. Li and G. Lei, *Energy Fuels*, 2022, **36**, 13296-13306.